Pages: 86-94 / Vol. 16/ Issue 2 / Summer- Fall 2023

Journal of Aerospace Science and Technology

www:jast.ias.ir

Scientific-Research Article

Space Robots Formation Control for Large Solar Sail Deployment

Mahshid Soleymani[1], **Maryam Kiani**[2]*

1-2- Department of Aerospace Engineering, Sharif University of Technology, Tehran, Iran

ABSTRACT

Solar sails use sunlight to propel a vehicle through space by reflecting solar photons off a mirror-like surface made of light-reflective material. To be able to work as an interplanetary cargo ship, the solar sail area should be large enough to receive the required acceleration from the sunlight. However, mechanical deploying mechanisms are not reliable for deploying such a large solar sail. This paper presents formation control of space robots for the on-orbit assembly of large solar sails. Contrary to previous works, the dynamic equations of space robots in the formation are derived by considering relative motion of the space robots concerning the sail hub orbiting the Earth. The uncertainties including external disturbances, unmolded dynamics, and parameter uncertainties, are considered a single time-varying term in the dynamic model. Then, an adaptive sliding mode controller combined with a second-order observer is expanded to control the on-orbit formation of space robots as well as resist the disturbances. Finally, a numerical simulation demonstrates the proposed approach is efficacy.

Keywords: *Solar Sail Assembly-Adaptive Sliding Mode Control-Formation Control*

Introduction

Solar sails are large, flexible, reflective surfaces that utilize solar radiation pressure to propel in space in a similar way that kites employ the wind to lift themselves up. They are accelerated by the momentum gained from the solar photons when they hit and reflect off the sail membrane [1]. Since the solar sails use solar energy, there is no need to supply propellant. Thus, they provide affordable propulsion, longer mission lifetimes, larger payload mass, access to unreachable orbits such as non-Keplerian and high solar latitude orbits, and high speeds in comparison with conventional propulsion systems [2]. Launched in 2010, Interplanetary Kite-craft Accelerated by Radiation of the Sun (IKAROS), made by the Japanese Aerospace Exploration Agency (JAXA), was solar sails were controlling the first demonstration of a spacecraft [3].

To be capable of carrying larger payloads and working as an interplanetary cargo-ship, the sail's area should be increased to receive more acceleration from the sunlight [4]. For instance, to carry a payload on the order of a few tons, a sail with an area of 1 km^2 is required [5]. But, for these ambitious flagship-class missions, there are some key technology challenges as follows [6]:

- Deployment of very large sail membranes
- Reducing areal density to the orders of 2.5-25 g/m^2
- Degradation of sail material due to the thermal effects and ultraviolet radiation
- Attitude control of deployed solar sail

1 PhD. Candidate

2 Assistant Professor (Corresponding Author) Email: * kiani@sharif.edu

doi.org/10.22034/jast.2023.404049.1157

Submit: 25.06.2023/ Accepted: 17.07/2023

Print ISSN:2345-3648 Online ISSN: 1735-2134

• Sail packing in a very efficient way

This paper focuses on the first issue, which is to provide an efficient solution for the deployment of the sail. Generally, a mechanical mechanism must be designed to deploy the solar sail automatically. However, most of the mechanisms, such as the spinning expansion devices [3] and deployable booms [7], are unreliable when the sail-craft size is in the orders of several kilometers. An efficient approach not affected by the system size is employing the on-orbit servicing robots to pull the sail to the desired position. Moreover, the space robots can be used for other missions including the assembly of the next solar sail after finishing their mission [4]. Bo and Gao [8] presented a sliding mode control approach for a formation consisting of two space robots in which a radial basis function-based neural network is employed to adjust the parameters of the control law. Queiroz et al. [9] developed a nonlinear adaptive controller to control the relative position of two spacecraft in a formation flying that overcomes the model uncertainties and external disturbances. Hu et al. [4] studied the on-orbit assembly of a 1 square kilometer solar sail employing a space robot formation. They proposed an adaptive sliding mode controller combined with a disturbance observer to control the formation of space robots. However, to simplify the dynamics and control problem, the formation of space robots has been considered a formation of ground robots. Therefore, the formation dynamic model is a set of four scalar linear equations corresponding to the motion of four robots.

This paper develops the dynamics and control problem of Ref. [4] for on-orbit formation of space robots that have been employed to deploy the large solar sail. Contrary to Ref. [4], the full nonlinear dynamics describing the relative motion of space robots in the formation flying is considered in this paper. The orbital dynamics of the solar sail is considered, and the motion of space robots on the solar sail is modeled as relative motion concerning the solar sail. Thus, the dynamic model of the space robot formation will be derived as vectorial nonlinear equations. Then, the adaptive sliding mode controller combined with the disturbance observer is expanded for the obtained model of the nonlinear multi input-multi output system.

The Dynamic Model of Space Robot Formation Flying

Sequence of on-orbit assembly of the solar sail

The solar sail consists of a hub that contains the wrapped sail before the extension, four booms as the supporting structure, and four wings in four quadrants as shown in Fig. 1 [4].
Each of the space robots has three manipulators that, by employing two of them it could move on the boom while holding the sail by the third one. During the on-orbit deployment of the sail, the first and second moments of mass of the sail, as well as the solar pressure and gravitational torques, will change dramatically due to the large size of the sail. Thus, in order to keep the solar sail attitude stable, the sequence of on-orbit assembly is considered, as shown in Fig. 2 [4]. The wings in the first and second quadrants are deployed at first, and then, the other wings in the third and fourth quadrants will be expanded.

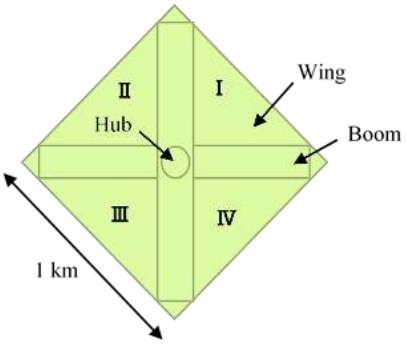

Fig. 1: The non-spinning solar sail

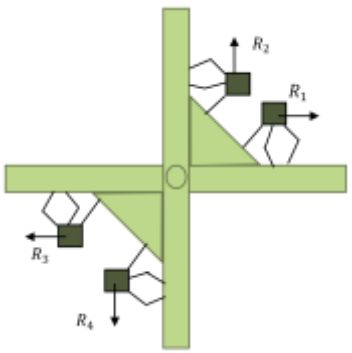

(a)

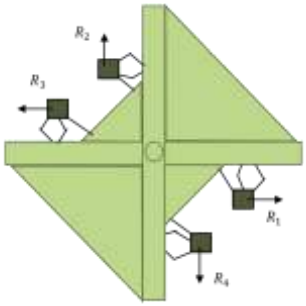

(b)

Fig. 2: The sequence of on-orbit deployment of the solar sail. (a) expanding the wing in quadrants I & III. (b) expanding the wing in quadrants II & IV.

Dynamic modeling

This subsection will derive a nonlinear dynamic model for the space robot formation. The leader-follower approach is considered for the formation. Firstly, the equations are developed for the relative motion of the fourth robot with respect to the on-orbit solar sail, and then, the relations are generalized for each of the space robots. R_4 is chosen as the leader and R_3 is its direct follower. Thus, the relative trajectory of R_4 with respect to the solar sail is the desired trajectory, and R_3 follows the actual trajectory of R_4. In the same way, $R_2$and R_1track the actual paths of R_3 andR_2, respectively. Moreover, the solar sail is assumed to be in a circular orbit around the Earth with a constant angular velocity ω. The schematic representation of the relative motion of the fourth space robot with respect to the solar sail is shown in Fig. 3.

According to Fig. 3, the following assumptions are made:

1. The inertial coordinate system XYZ is attached to the center of the earth.
2. $\vec{R}(t) \in \mathbb{R}^3$ is the position vector from the inertial frame's center to the solar sail's center.
3. The coordinate frame $x_s y_s z_s$ is attached to the solar sail hub so that the x_s axis is in the opposite direction of tangential velocity, the y_s axis along the $\vec{R}$ vector, and the z_s axis perpendicular to x_s and y_s establish a right-handed coordinate system.
4. $\vec{\rho}(t) \in \mathbb{R}^3$ is the relative position vector from the origin of the solar sail coordinate system to the space robot R_4.

The nonlinear dynamic equations of the solar sail and space robot R_4 with respect to the inertial frame XYZ are respectively written as follows:

$$m_s\ddot{\vec{R}} + m_s(M+m_s)G\left(\vec{R}/\|\vec{R}\|^3\right) = \vec{u}_s + \vec{F}_s^d \qquad (1)$$

$$m_{R4}(\ddot{\vec{R}} + \ddot{\vec{\rho}}) + m_{R4}(M+m_{R4})G\left((\vec{R}+\vec{\rho})/\|\vec{R}+\vec{\rho}\|^3\right) = \vec{F}_{R4}^c + \vec{F}_{R4}^d \qquad (2)$$

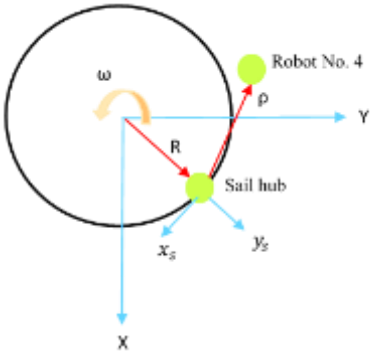

Fig. 3: schematic representation of the relative motion of the fourth space robot with respect to the solar sail from the top view.

Where m_s and m_{R4} are masses, $\vec{F}_{ds}, \vec{F}_{dR4} \in \mathbb{R}^3$ are disturbing force vectors, and $\vec{u}_s(t), \vec{u}_{R4}(t) \in \mathbb{R}^3$ are controlling force vectors for the solar sail and space robot R_4, respectively. Also, M and G are the Earth's mass and the universal gravity constant, respectively. Due to the fact that $M \gg m_s, m_{R4}$, the Eqs. (1) and (2) are simplified as follows:

$$m_s\ddot{\vec{R}} + m_s\mu\left(\vec{R}/\|\vec{R}\|^3\right) = \vec{u}_s + \vec{F}_s^d \qquad (3)$$

$$m_{R4}(\ddot{\vec{R}} + \ddot{\vec{\rho}}) + m_{R4}\mu\left((\vec{R}+\vec{\rho})/\|\vec{R}+\vec{\rho}\|^3\right) = \vec{F}_{R4}^c + \vec{F}_{R4}^d \qquad (4)$$

Where $\mu = 398600\ km^3/s^2$ is the standard gravitational parameter. After applying some algebraic simplifications on Eqs. (3) and (4), the describing dynamic equation of the space robot R_4 with respect to the solar sail expressed in the XYZ coordinate system is written as follows:

$$m_{R4}\ddot{\vec{\rho}} + m_{R4}\mu\left(\frac{\vec{R}+\vec{\rho}}{\|\vec{R}+\vec{\rho}\|^3} - \frac{\vec{R}}{\|\vec{R}\|^3}\right) = \vec{F}_{R4}^c + \frac{m_{R4}}{m_s}\vec{u}_s + \vec{F}_{R4}^d - \frac{m_{R4}}{m_s}\vec{F}_s^d \qquad (5)$$

In order to express the Eq. (5) in the coordinate $x_s y_s z_s$ system, first it should be noted that the relative position vector $\vec{\rho}(t)$ is written as follows in the $x_s y_s z_s$ coordinate system:

$$\vec{\rho} = x\hat{\imath}_s + y\hat{\jmath}_s + z\hat{k}_s \qquad (6)$$

Also, the constant angular velocity vector ω equals $\omega\hat{k}_s$. Thus, the relative acceleration $\ddot{\vec{\rho}}(t)$ is written in the following form:

$$\ddot{\vec{\rho}} = (\ddot{x} - 2\omega\dot{y} - \omega^2 x)\hat{\imath}_s + (\ddot{y} + 2\omega\dot{x} - \omega^2 y)\hat{\jmath}_s + \ddot{z}\hat{k}_s \quad (7)$$

Moreover, the vector $\vec{R} = \|\vec{R}\|\hat{\jmath}_s$ is constant in the moving coordinate system $x_s y_s z_s$. By substituting the right-hand side of Eq. (7) into the Eq. (5), the nonlinear dynamic equation of the space robot R_4 with respect to the solar sail is:

$$m_{R4}\ddot{\vec{q}} + C(\omega)\dot{\vec{q}} + N(\vec{q}, \omega, \vec{R}, \vec{u}_s) = \vec{F}^c_{R4} + \vec{F}^d_{R4} \quad (8)$$

Where the relative position vector $\vec{q}(t) \in \mathbb{R}^3$ is equal to:

$$\vec{q}(t) = [x(t) \quad y(t) \quad z(t)]^T \quad (9)$$

The Coriolis matrix $C(\omega) \in \mathbb{R}^{3\times3}$ is as follows:

$$C(\omega) = 2m_{R4}\omega \begin{bmatrix} 0 & -1 & 0 \\ 1 & 0 & 0 \\ 0 & 0 & 0 \end{bmatrix} \quad (10)$$

$N(.) \in \mathbb{R}^3$ is a nonlinear expression that is defined in the following form:

$$N(\vec{q}, \omega, \vec{R}, \vec{u}_s) = \begin{bmatrix} m_{R4}\mu \dfrac{x}{\|\vec{R}+\vec{q}\|^3} - m_{R4}\omega^2 x + \dfrac{m_{R4}}{m_s}u_{sx} \\ m_{R4}\mu\left(\dfrac{y+\|\vec{R}\|}{\|\vec{R}+\vec{q}\|^3} - \dfrac{1}{\|\vec{R}\|^2}\right) - m_{R4}\omega^2 y + \dfrac{m_{R4}}{m_s}u_{sy} \\ m_{R4}\mu \dfrac{z}{\|\vec{R}+\vec{q}\|^3} + \dfrac{m_{R4}}{m_s}u_{sz} \end{bmatrix} \quad (11)$$

Also, $\vec{F}_d \in \mathbb{R}^3$ in Eq. (8) is the disturbance force vector that is defined as $\vec{F}_{dR4} = -\mu_{R4}\dot{\vec{q}}_{R4}$.

So far, the nonlinear dynamic equation of R_4 has been achieved. The equation of motion of the space robot formation is obtained in the following form:

$$m_n\ddot{\vec{q}} + C(\omega)\dot{\vec{q}} + N(\vec{q}, \omega, \vec{R}, \vec{u}_s) = \vec{F}^c_n + \vec{F}^d_n \quad n = 1,2,3,4 \quad (12)$$

Controller Design

Control Objective

Knowing the desired path $\vec{q}_d(t) \in \mathbb{R}^3$ for the leader space robot R_4 concerning the solar sail, the control objective is described as follows:

$$\lim_{t\to\infty} \vec{e}_n = 0 \quad (13)$$

Where,

$$\vec{e}_n(t) = \vec{q}^d_n(t) - \vec{q}_n(t) \quad n = 1,2,3,4 \quad (14)$$

The desired acceleration of robot R_4 for $t < T$ is chosen to be:

$$\ddot{\vec{q}}^d_{R4} = [A\sin(2\pi t/T) \quad A\cos(2\pi t/T) \quad 0]^T \quad (15)$$

The desired acceleration is considered to be zero anywhere else. In Eq. (15), A and T are equal to 1.8×10^{-3} and 1500, respectively.

Adaptive sliding mode control formulation

In this subsection, the proposed controller of Ref. [4] will be modified to control the on-orbit formation of space robots. The system dynamics (Eq. (12)) is rewritten assuming no control over the solar sail, i. e. $\vec{u}_s = 0$, as follows:

$$m_n\ddot{x} - 2m_n\omega\dot{y} + m_n\mu\frac{x}{\|\vec{R}+\vec{r}\|^3} - m_n\omega^2 x = F^c_{nx} + F^d_{nx} \quad (16)$$

$$m_n\ddot{y} + 2m_n\omega\dot{x} + m_n\mu\left(\frac{y+\|\vec{R}\|}{\|\vec{R}+\vec{r}\|^3} - \frac{1}{\|\vec{R}\|^2}\right) - m_n\omega^2 y = F^c_{ny} + F^d_{ny} \quad (17)$$

$$m_n\ddot{z} + m_n\mu\frac{z}{\|\vec{R}+\vec{r}\|^3} = F^c_{nz} + F^d_{nz} \quad (18)$$

As it can be seen from the above relations, the control force must be applied in any direction. It is clear from the Eqs. (16)-(18) that we are dealing with a multi-input-multi-output system. Since there is a control in each direction, a sliding surface must be defined for each input. Therefore, there is a controller for each space robot that should apply the control law in each direction. The sliding surfaces are chosen as follows:

$$\vec{S}_n = [\dot{e}_{nx} + \lambda e_{nx} \quad \dot{e}_{ny} + \lambda e_{ny} \quad \dot{e}_{nz} + \lambda e_{nz}]^T \quad (19)$$

Where λ is a positive constant. The control law in each direction is written in the following form:

$$\vec{u}_n = \begin{bmatrix} -K_D S_{nx} - \lambda\dot{e}_{nx} - (\varepsilon_{0x} + \hat{\varepsilon}_x)sign(S_x) \\ -K_D S_{ny} - \lambda\dot{e}_{ny} - (\varepsilon_{0y} + \hat{\varepsilon}_y)sign(S_y) \\ -K_D S_{nz} - \lambda\dot{e}_{nz} - (\varepsilon_{0z} + \hat{\varepsilon}_z)sign(S_z) \end{bmatrix} \quad (20)$$

In which, $K_D > 0$, and $\hat{\varepsilon}$ is updated by the following differential equations [4]:

$$\dot{\hat{\varepsilon}}_n = \begin{bmatrix} \frac{1}{\kappa}(-\tau\hat{\varepsilon}_{nx} + |S_{nx}|) \\ \frac{1}{\kappa}(-\tau\hat{\varepsilon}_{ny} + |S_{ny}|) \\ \frac{1}{\kappa}(-\tau\hat{\varepsilon}_{nz} + |S_{nz}|) \end{bmatrix} \quad (21)$$

In which, $\kappa > 0$ is the sensitivity coefficient of $\hat{\varepsilon}$. The smaller the κ is, the more sensitive the $\dot{\hat{\varepsilon}}$ is to $|S|$. Also, $\tau > 0$ is a small constant so that the expression $-\tau\hat{\varepsilon}$ causes $\hat{\varepsilon}$ remain a small constant when $|S|$ is in the neighborhood of zero. Moreover, In Eq. (20), $\varepsilon_0 > 0$ is the constant part of the adaptive gain $(\varepsilon_0 + \hat{\varepsilon})$ as well as sets the minimum uncertainty tolerance capability for the controller.

To avoid chattering, *sign(S)* can be replaced with the hyperbolic tangent function [4], which results in the following relationships.

$$\vec{u}_n = \begin{bmatrix} -K_D S_{nx} - \lambda\dot{e}_{nx} - (\varepsilon_{0x} + \hat{\varepsilon}_x)tanh(\eta S_x) \\ -K_D S_{ny} - \lambda\dot{e}_{ny} - (\varepsilon_{0y} + \hat{\varepsilon}_y)tanh(\eta S_y) \\ -K_D S_{nz} - \lambda\dot{e}_{nz} - (\varepsilon_{0z} + \hat{\varepsilon}_z)tanh(\eta S_z) \end{bmatrix} \quad (22)$$

Where the scalar η determines the similarity between $tanh(\eta S)$ and sign*(S)*.

Eventually, the actual control forces are computed by the following relations:

$$\vec{F}_n^c = \begin{cases} m_n(\ddot{\vec{q}}_n^d - \vec{u}_n) + C(\omega)\dot{\vec{q}}_n + N(\vec{q}, \omega, \vec{R}), \\ n = N \\ \vec{F}_{n+1}^c - \vec{u}_n, n = N-1, \dots, 1 \end{cases} \quad (23)$$

Disturbance observer

As can be seen from Eq. (22), measuring the translational velocity of space robots is required. However, obtaining the velocity information of a maneuvering space robot is difficult and even measurement noise will be added to the system. Therefore, to improve the controller performance, the second-order observer with finite time convergence [4], [10] is modified to estimate disturbance in any direction for each space robot and compensate for it in the controller. The block diagram of the controller combined with the second-order observer is shown in Fig. 4. Note that the inputs and outputs of the blocks in Fig. 4 are vectors contrary to Ref. [4].

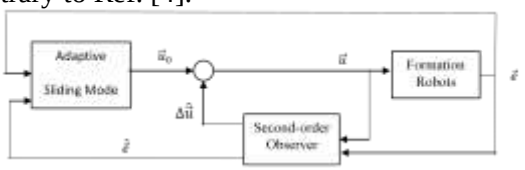

Fig. 4: block diagram of the controller combined with the second-order observer.

According to Eq. (14), to adapt the observer for the problem considered in this paper, the error dynamics can be written as follows:

$$\vec{e}_n(t) = \vec{q}_n^d(t) - \vec{q}_n(t) = \vec{q}_n^d(t) - \frac{1}{m_n}\left(-C(\omega)\dot{\vec{q}}_n - N(\vec{q}, \omega, \vec{R}) + \vec{F}_n^c + \vec{F}_n^d\right) \quad n = 1, \dots, 4 \quad (24)$$

Without loss of generality, it is assumed that the masses of space robots are $m_n = 1$ and $\Delta\vec{\rho}_n = -\vec{F}_n^d$ as well as $\vec{u}_n = \ddot{\vec{q}}_n^d - \vec{F}_n^c$. To rewrite the error dynamics in state space form, the following variables are considered:

$$\begin{cases} \vec{x}_1 = \vec{e}_n \\ \vec{x}_2 = \dot{\vec{e}}_n \\ \Delta\vec{u} = \Delta\vec{\rho}_n \\ \vec{u} = \vec{u}_n \end{cases} \quad (25)$$

So, we have:

$$\begin{cases} \dot{\vec{x}}_1 = \vec{x}_2 \\ \dot{\vec{x}}_2 = \Delta\vec{u} + \vec{u} \end{cases} \quad (26)$$

The second-order observer is considered as follows:

$$\begin{cases} \dot{\hat{\vec{x}}}_{1n} = \vec{\chi}_{1n} \\ \vec{\chi}_{1n} = \hat{\vec{x}}_{2n} - \gamma_3\left|\hat{\vec{x}}_{1n} - \vec{x}_{1n}\right|^{2/3} \times sign(\hat{\vec{x}}_{1n} - \vec{x}_{1n}) \\ \dot{\hat{\vec{x}}}_{2n} = \vec{u}_n + \Delta\hat{\vec{u}}_n \\ \Delta\hat{\vec{u}}_n = -\gamma_2\left|\hat{\vec{x}}_{2n} - \vec{\chi}_{1n}\right|^{1/2} \times sign(\hat{\vec{x}}_{2n} - \vec{\chi}_{1n}) + \hat{\vec{x}}_{3n} \\ \dot{\hat{\vec{x}}}_{3n} = -\gamma_1 \times sign(\hat{\vec{x}}_{3n} - \Delta\hat{\vec{u}}_n) \end{cases} \quad (27)$$

In the Eq. (27), $\hat{\vec{x}}_1, \hat{\vec{x}}_2, \Delta\hat{\vec{u}}$, and $\hat{\vec{x}}_3$ are the observed values of $\vec{x}_1, \vec{x}_2, \Delta\vec{u}$, and $\vec{u}$, respectively. Also, γ_1, γ_2, and γ_3 are constants to be chosen.

Note that the above observer should be employed for any space robot in each direction. For this reason, the relations in Eq. (27) are vector.

Simulation and Results

In order to simulate the problem, the system dynamics is represented in the state space form for $n = 1,2,3,4$:

$$\begin{Bmatrix} \dot{\vec{q}}_{1n} \\ \dot{\vec{q}}_{2n} \end{Bmatrix} = \begin{Bmatrix} \vec{q}_{2n} \\ \frac{\vec{F}_n^c + \vec{F}_n^d - C\vec{q}_{2n} - N}{m_n} \end{Bmatrix} \quad (28)$$

Where $\vec{F}_n^d = -\mu_n\dot{\vec{q}}_n$, $\mu_1 = 0.56, \mu_2 = 0.48$, $\mu_3 = 0.32$, and $\mu_4 = 0.65$. The simulation parameters have been reported in Table 1.

Table 1: Simulation parameters.

parameters	value
K_D	2
λ	5
ε_0	0.001
κ	10
τ	0.01
η	10

The masses of robots are equal to $m_1 = m_2 = m_3 = m_4 = m_{real} = 200\ kg$ in the dynamic model. To examine the robustness of the presented method in the presence of parametric uncertainties, it is assumed 20% mass uncertainty in the controller. Thus, we have $m_1 = m_2 = m_3 = m_4 = 1.2m_{real} = 240\ kg$.

Results and discussion

In the following, the actual and desired paths are drawn in a graph for each robot to compare.

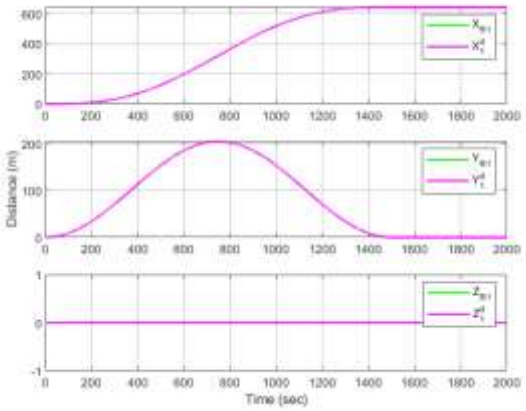

Fig. 5: The actual and desired paths for space robot 1 along x direction, y direction, and z direction.

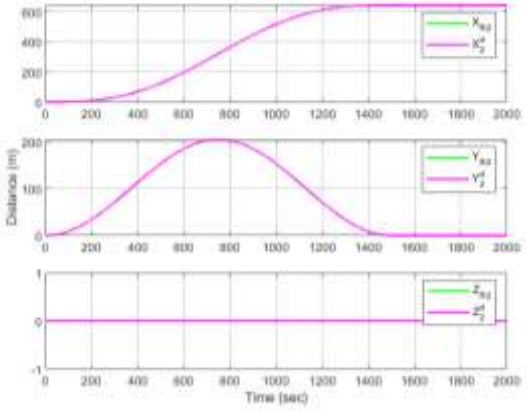

Fig. 6: The actual and desired paths for space robot 2 along x, y, and z directions.

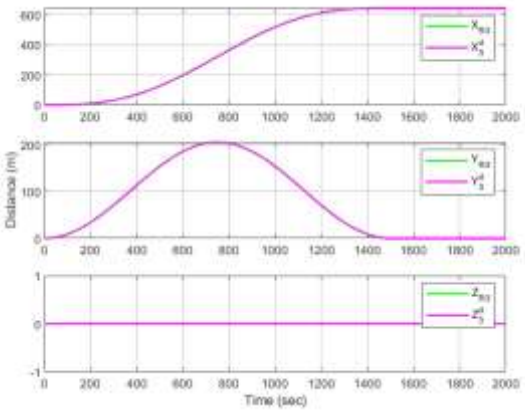

Fig. 7: The actual and desired paths for space robot 3 along x direction, y direction, and z direction.

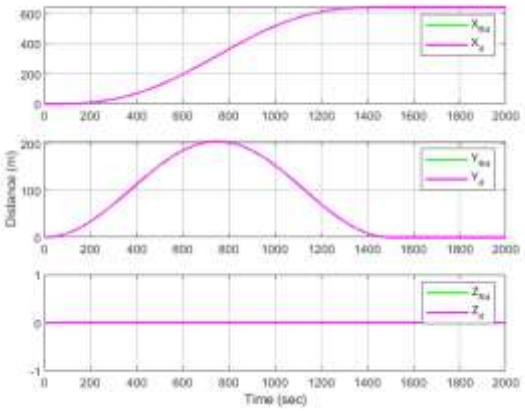

Fig. 8: The actual and desired paths for space robot 4 along x direction, y direction, and z direction.

The tracking error of desired path for each of the space robots along x, y, and z direction is drawn in Figs. 9-12.

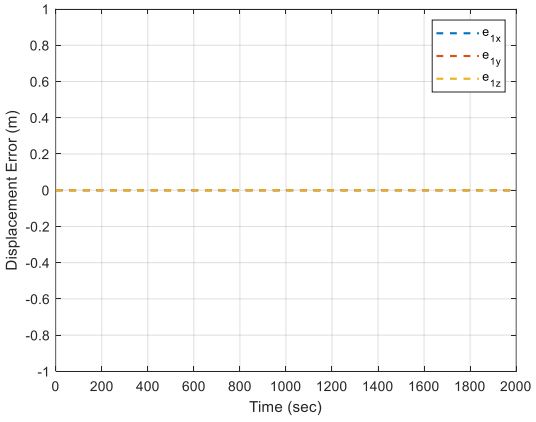

Fig. 9: The tracking error for space robot 1.

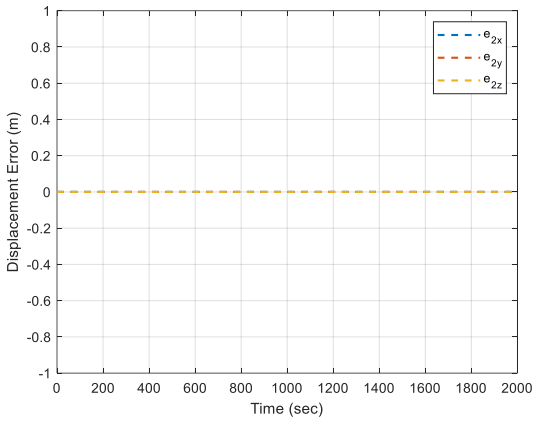

Fig. 10: The tracking error for space robot 2.

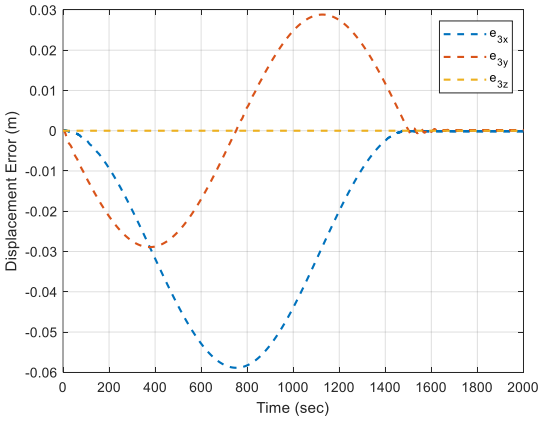

Fig. 11: The tracking error for space robot 3.

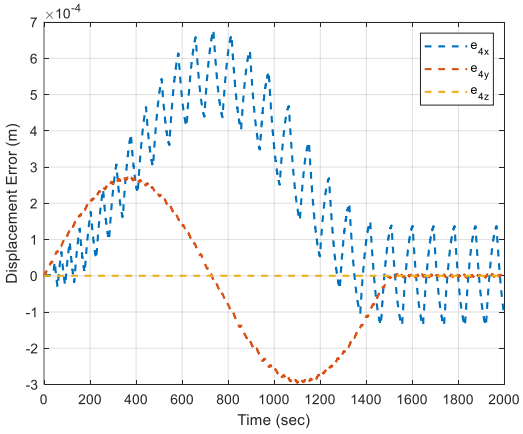

Fig. 12: The tracking error for space robot 4.

The control forces of the space robots are shown in Figs. 13-16.

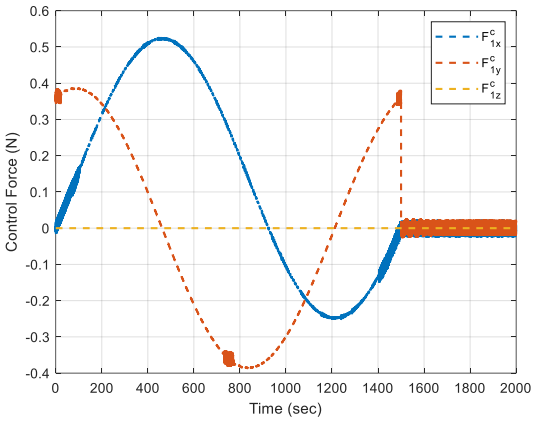

Fig. 13: The control force of the space robot 1.

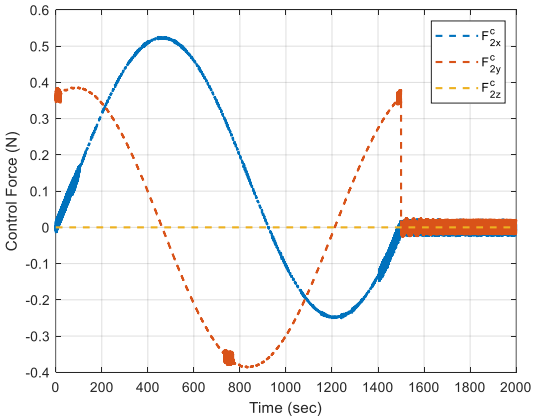

Fig. 14: The control force of the space robot 2.

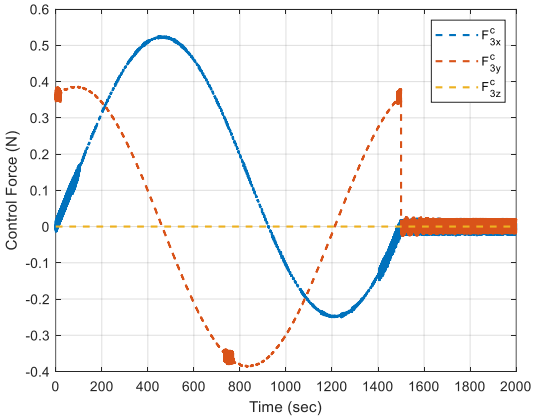

Fig. 15: The control force of the space robot 3.

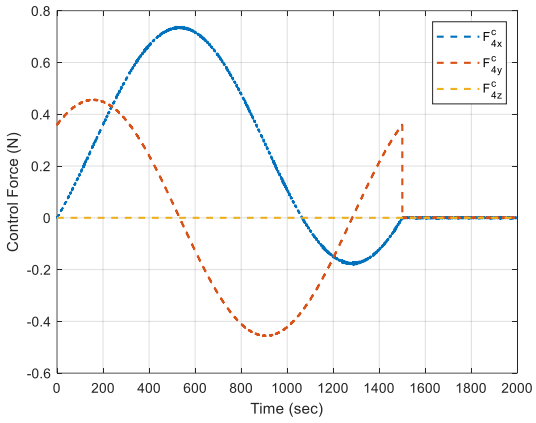

Fig. 16: The control force of the space robot 4.

As it can be seen from the Figs. 9-12, the controller truly realizes the control objective. The trajectory tracking error of the fourth robot is on the order of 10^{-4} meter i. e., 0.1 millimeters as well as for the third robot it is on the order of a centimeter. Also, as it is clear from the Figs. 5-8, all of the space robots have tracked the desired path well.

Concluding Remarks and Future Work

This paper presents the formation control of space robots in order to on-orbit assembly of large solar sails. The full nonlinear dynamic model of the formation consisting of four on-orbit space robots is derived using the leader-follower approach. Then, an adaptive sliding mode controller is developed for the derived model. Moreover, a second-order observer is embedded in the system to overcome the uncertainties, including the unmolded dynamics, parameter uncertainties, and external disturbances. Eventually, simulation results indicate that the space robots accurately track the desired trajectory to deploy the solar sail. Future works will focus on considering the attitude control of the solar sail during the assembly of the sail and the flexibility of the supporting booms.

References

[1] J. Baculi and M. A. Ayoubi, “Fuzzy attitude control of solar sail via linear matrix inequalities,” *Acta Astronautica*, vol. 138, pp. 233–241, Sep. 2017.
[2] B. Wie and D. Murphy, “Solar-sail attitude control design for a flight validation mission,” *Journal of Spacecraft and Rockets*, vol. 44, no. 4, pp. 809–821, Jul 2007.
[3] Y. Tsuda and et al., “Flight status of IKAROS deep space solar sail demonstrator,” *Acta Astronautica*, vol. 69, pp. 833–840, Nov. 2011.
[4] Q. Hu, and et al., “Formation control of multi-robots for on-orbit assembly of large solar sails,” *Acta Astronautica*, vol. 123, pp. 446–454, Jun. 2016.
[5] B. Fu, and F. O. Eke., “Attitude control methodology for large solar sails,” *Journal of Guidance, Control, and Dynamics*, vol. 38, no. 4. pp. 662–670, Apr. 2015.
[6] D. A. Spencer, and et al., “Solar sailing technology challenges,” *Aerospace Science and Technology*, vol. 93, pp. 105276, Oct. 2019.
[7] B. Woo, and et al., “Deployment experiment for ultralarge solar sail system (ultrasail),” *Journal of Spacecraft and Rockets*, vol. 48, no. 5, pp. 874-880, Sep. 2011.
[8] X. Bo, and Y. Gao, “"Sliding mode control of space robot formation flying,” in *2009 IEEE International Conference on Autonomous Robots and Agents*, Wellington, New Zealand, 2009, pp. 561–565.
[9] M. S. De Queiroz, and et al., “Adaptive nonlinear control of multiple spacecraft formation flying,” *Journal of Guidance, Control, and Dynamics*, vol. 23, no. 3, pp. 385-390, May. 2000.
[10] L. Fridman, and A. Levant, “Higher order sliding modes,” *Sliding mode control in engineering* , vol. 11, pp. 53-102, Jan. 2002.